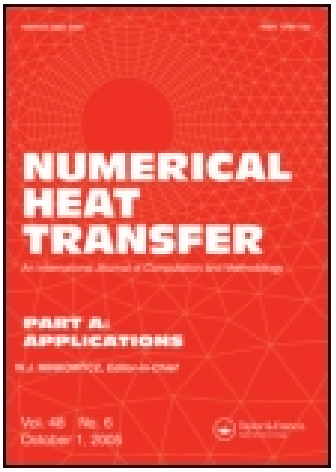


Numerical Heat Transfer, Part A: Applications: An International Journal of Computation and Methodology

Publication details, including instructions for authors and subscription information:
http://www.tandfonline.com/loi/unht20

# Laminar Free Convection in a Square Enclosure Driven by the Lorentz Force

I. E. Sarris [a] , D. G. E. Grigoriadis [b] & N. S. Vlachos [a]

[a] Department of Mechanical Engineering , University of Thessaly , Volos, Greece

[b] Department of Mechanical and Manufacturing Engineering , University of Cyprus , Nicosia, Cyprus

Published online: 06 Dec 2010.

To cite this article: I. E. Sarris , D. G. E. Grigoriadis & N. S. Vlachos (2010) Laminar Free Convection in a Square Enclosure Driven by the Lorentz Force, Numerical Heat Transfer, Part A: Applications: An International Journal of Computation and Methodology, 58:12, 923-942, DOI: 10.1080/10407782.2010.529034

To link to this article: http://dx.doi.org/10.1080/10407782.2010.529034

*Numerical Heat Transfer, Part A*, 58: 923–942, 2010

ISSN: 1040-7782 print/1521-0634 online
DOI: 10.1080/10407782.2010.529034

Taylor & Francis
Taylor & Francis Group

# LAMINAR FREE CONVECTION IN A SQUARE ENCLOSURE DRIVEN BY THE LORENTZ FORCE

**I. E. Sarris[1], D. G. E. Grigoriadis[2], and N. S. Vlachos[1]**
[1]*Department of Mechanical Engineering, University of Thessaly, Volos, Greece*
[2]*Department of Mechanical and Manufacturing Engineering, University of Cyprus, Nicosia, Cyprus*

***A numerical study is presented of laminar free convection flow driven by magnetic forces. An external magnetic field with one spatially varying component is applied to an electrically conducting fluid in a square enclosure. This magnetically-driven flow is controlled by the intensity and the wave number of the applied magnetic forcing. In addition, when the enclosure is heated laterally in a non-zero gravity environment, the resulting buoyant forces may contribute or resist the magnetically-driven fluid motion. The present results show that a strong magnetic field can even reverse the buoyant flow. The circulation intensity of the flow and the heat transfer from the sidewalls is increased with increasing magnetic field or with decreasing magnetic Reynolds number. The wave number of the magnetic forcing is also an important parameter that determines the vortex patterns and, consequently, the convection heat transfer.***



## 1. INTRODUCTION

The usual effect of a uniform external magnetic field applied to a natural convection flow is to decelerate the fluid motion and to reorganize the flow patterns [1–4]. The dumping effect of the magnetic field on convection flow helps in the production of crystals (Bridgman and Czochralski installations [5, 6]), while undesirable turbulent phenomena in metal casting and transport could be minimized [7, 8]. On the other hand, the reduction of the convection heat transfer of liquid metals in the blanket of thermonuclear fusion reactors may be cited as an example of undesired magnetic dumping effect. This is because it reduces the ability of the blanket to handle the large heat quantities that must be transferred from the core reactor

Received 9 December 2009; accepted 10 September 2010.

The suggestion of Prof. Daniele Carati of ULB to focus on MHD fluid flows driven by a nonuniform magnetic field is gratefully acknowledged. The authors also thank Dr. Alkis Grecos for fruitful discussions. This work was performed in the framework of the EURATOM—Hellenic Republic Association and is supported by the European Union within the Fusion Program. The content of this publication is the sole responsibility of the authors and it does not necessarily represent the views of the Commission or its services.

Address correspondence to N. S. Vlachos, Department of Mechanical Engineering, University of Thessaly, Athens Avenue 38334 Volos, Greece. E-mail: vlachos@mie.uth.gr

## NOMENCLATURE

| | |
|---|---|
| $\mathbf{B}$ | magnetic field vector |
| $B_x$, $B_y$ | dimensionless magnetic field components |
| $c_P$ | specific heat |
| $F$ | Lorentz force |
| $g$ | gravitational acceleration |
| Gr | Grashof number |
| $H$ | enclosure height |
| Ha | Hartmann number |
| $j$ | current density |
| $\mathbf{J}$ | dimensionless current density |
| $k$ | wave number of the sinusoidal magnetic forcing |
| Nu | Nusselt number |
| $p$ | fluid pressure |
| $p'$ | total pressure |
| $P$ | dimensionless pressure |
| Pr | Prandtl number |
| $R_m$ | magnetic Reynolds number |
| $T$ | fluid temperature |
| $t$ | time |
| $u$, $v$ | velocity components in $x$ and $y$ directions |
| $U$, $V$ | dimensionless velocity components |
| $\mathbf{V}$ | velocity field vector |
| $x$, $y$ | spatial coordinates |
| $X$, $Y$ | dimensionless coordinates |
| $\alpha$ | thermal diffusivity |
| $\beta$ | coefficient of thermal expansion |
| $\Delta T$ | temperature difference of sidewalls |
| $\epsilon$ | convergence criterion |
| $\Theta$ | dimensionless temperature |
| $\mu$ | magnetic permeability |
| $\nu$ | fluid kinematic viscosity |
| $\rho$ | fluid density |
| $\sigma$ | fluid electrical conductivity |
| $\phi$ | generalized variable |
| $\Psi$ | nondimensional stream function |

***Subscripts and superscripts***

| | |
|---|---|
| $c$ | cold |
| $h$ | hot |
| $n$ | iteration number or time |
| max | maximum |
| $x$, $y$, $z$ | Cartesian coordinate indices |
| 0 | reference value |



[9]. The reason for fluid deceleration in these applications by the magnetic field is the action of the so-called Lorentz force that resists the fluid motion.

In general, the Lorentz force is proportional to the product of the parameter $\frac{\mathrm{Ha}^2}{R_m}$ and the vector product $\mathbf{B}\nabla\mathbf{B}$ (where Ha is the Hartmann number, $R_m$ is the magnetic Reynolds number, and $\mathbf{B}$ is the magnetic field). In the case of a uniform magnetic field, the Lorentz force is always opposite to the fluid velocity vector, thus dumping the flow and exists only in moving fluids. On the contrary, in the case of a suitable spatially nonuniform external magnetic field, the Lorentz force can even be the driving force for the fluid flow. For example, the Lorentz force which is applied through the divergence-free external magnetic field $\mathbf{B}(B_x, B_y \sin k\pi x, 0)$ that is produced with the suitable application of current electrodes and permanent magnets is of the type

$$F = B_x B_y k\pi \cos k\pi x \tag{1}$$

which clearly has a rotational action on the fluid even when at rest.

The present magnetohydrodynamic (MHD) spatially periodic two-dimensional flow with magnetic forcing is used primarily in laboratory experiments. The first successful attempt in this direction is due to Bondarenko et al. [10] and Batchaev and Dowzhenko [11] who realized a flow with similar forcing in a layer of an electrically conducting fluid driven by electromagnetic fields. A review of laboratory realizations of the present flow can also be found in Obukhov [12]. These experiments showed that the first flow instability leads to a stationary secondary flow pattern with

a wave number different from the basic flow. As the electric current is increased, the flow undergoes a Hopf bifurcation resulting in an oscillatory state, with chaotic behavior of the flow patterns. Thus, it is found that the resulting rotating flow (a Kolmogorov flow due to magnetic forcing) can be in the laminar, transitional or fully turbulent regime depending on the strength of the electric or magnetic field. The stability of this flow has been studied by Thess [13] for the two-dimensional basic flow, while fully turbulent three-dimensional simulations can be found in references [14–16].

An alternative configuration of the same flow was presented in the magneto–hydrodynamic experiment performed by Honji [17] where a vertical magnetic field is locally produced in the vicinity of a long lateral wall by permanent magnets placed below the bottom of the enclosure. An electric current is passed through the electrolyte from one short side of the enclosure to the other. Each magnet can produce a constant magnetic field and the magnets are put together to form a line of alternated poles. The fluid is, thus, subjected to an electromagnetic force, stationary in time and periodic in space, and the resulting flow is a localized linear array of alternating vortices. The spatio-temporal dynamics of this forced periodic flow due to electromagnetic forces in a confined domain was studied by Nakamura [18].

In the present work, a laterally-heated square enclosure with infinite extent in the third direction is considered. The imposed magnetic field generates the driving force of the convective flow of the electrically conducting fluid. The important flow parameters to be defined below are the Hartmann number, the wave number of the Lorentz force, and the magnetic Reynolds number. In addition to the magnetic forces, the buoyancy forces due to a temperature difference between the isothermal sidewalls is considered. It should be noted that the hydrodynamic stability of the stratified two-dimensional Kolmogorov flow was studied numerically by Balmforth and Young [19, 20]. However, to the authors knowledge this is the only numerical study of convection flow in enclosures driven both by a nonuniform Lorentz force of Kolmogorov forcing type and by a buoyancy force. This is the reason that the present study is restricted only to the laminar flow regime, as the primary goal is to identify the basic kinematic and heat transfer mechanisms.



## 2. PROBLEM SETUP

A laterally-heated square enclosure with electrically-insulated walls, as shown in Figure 1, is subjected to an external magnetic field **B** with components $(B_o,\ B_o \sin k\pi x,\ 0)$. A rotational Lorentz force due to the external magnetic field is developing on the electrically-conducting fluid that fills the enclosure and a circulating flow is started. The Lorentz force acting on the fluid when at rest is of the type $B_o^2 k\pi \cos k\pi x$, which may be modified by possible magnetic and kinetic fluctuations. Thus, the magnetic energy upon stationarity is transformed by the Lorentz force to fluid kinetic energy. The horizontal walls of the enclosure are considered adiabatic, while the isothermal vertical sidewalls are kept at a constant temperature difference, $\Delta T = T_c - T_h$, with $T_c$, $T_h$ being the temperatures of the cold and hot sidewall, respectively.

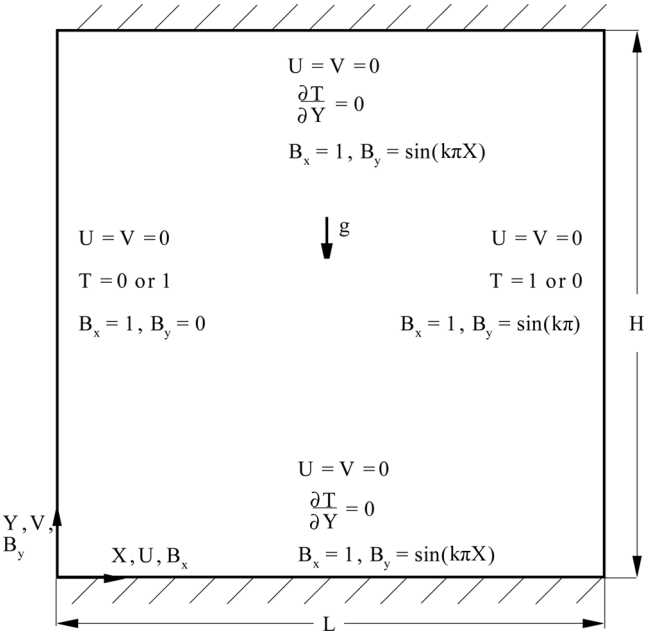


**Figure 1.** Flow configuration and boundary conditions.

Using as characteristic length the height of the enclosure, $H$, and as characteristic velocity the viscous scale, $\frac{\nu}{H}$, the nondimensional variables read as

$$\begin{aligned} \tau &= \frac{t\nu}{H^2}, \quad X = \frac{x}{H}, \quad Y = \frac{y}{H}, \\ U &= \frac{uH}{\nu}, \quad V = \frac{vH}{\nu}, \quad \Theta = \frac{T - T_c}{\Delta T}, \\ \mathbf{B}' &= \frac{\mathbf{B}}{B_0}, \quad \mathbf{J} = \frac{B_0}{\mu H}\mathbf{j}, \quad P = \frac{p\prime H^2}{\rho\nu^2}, \end{aligned} \tag{2}$$

where $\rho$ is the fluid density, $p'$ is the total pressure which includes also the magnetic pressure (i.e., $p' = p + \frac{1}{2\mu}B^2$), $\nu$ is the kinematic viscosity, (**j**) the current density, and $\mu$ is the magnetic permeability of the vacuum.

The nondimensional governing equations of momentum, magnetic induction, and thermal energy then read as

$$\partial_t \mathbf{V} + \mathbf{V}\nabla\mathbf{V} = -\nabla\mathbf{P} + \nabla^2\mathbf{V} + \mathrm{Gr}\Theta + \frac{\mathrm{Ha}^2}{R_m}\mathbf{B}\nabla\mathbf{B} \tag{3}$$

$$\partial_t \mathbf{B} + \mathbf{V}\nabla\mathbf{B} = \frac{1}{R_m}\nabla^2\mathbf{B} + (\mathbf{B}\nabla)\mathbf{V} \tag{4}$$

$$\partial_t \Theta + \mathbf{V}\nabla\Theta = \frac{1}{\mathrm{Pr}}\nabla^2\Theta \tag{5}$$

where the prime has been dropped from $\mathbf{B}'$.

The above set of equations is solved together with the equation of mass continuity $\nabla\cdot\mathbf{V}=0$, while an additional equation, $\nabla\cdot\mathbf{B}=0$, is used to verify that the magnetic field $\mathbf{B}$ is divergence-free. For the present laminar simulations, the use of divergence-free initial and boundary conditions for the magnetic induction was adequate to keep the residuals of this divergence in the order of the truncation error.

The nondimensional parameters of the flow are the Hartmann number $\mathrm{Ha}=B_0H\sqrt{\frac{\sigma}{\rho\nu}}$, the magnetic Reynolds number $R_m=\sigma\mu\nu$, the Grashof number $\mathrm{Gr}=\frac{g\beta\Delta TH^3}{\nu^2}$, and the Prandtl number $\mathrm{Pr}=\frac{\nu}{\alpha}$, where $g$ is the gravity acceleration, $\beta$ is the volumetric thermal expansion coefficient, $\alpha$ is the thermal diffusivity, and $\sigma$ is the electric conductivity of the liquid metal.

The initial and boundary conditions for the velocity, temperature, and magnetic induction are

$$\begin{aligned}
&\tau=0\\
&U=V=\Theta=B_x=B_y=0\\
&\tau>0\\
&U=V=0,\quad \frac{\partial\Theta}{\partial Y}=0\quad \text{for } Y=0,1\\
&U=V=0,\quad \Theta=0\text{ or }1\quad \text{for } X=0\\
&U=V=0,\quad \Theta=1\text{ or }0\quad \text{for } X=1\\
&B_x=1\quad \text{for } X=0,1\quad Y=0,1\\
&B_y=\sin k\pi X\quad \text{for } X=0,1\quad Y=0,1
\end{aligned}\tag{6}$$

The intensity of flow rotation inside the enclosure may be measured by the streamfunction $\Psi$: $U=\frac{\partial\Psi}{\partial Y}$ or $V=-\frac{\partial\Psi}{\partial X}$. A reference value $\Psi=0$ for the integration of the streamfunction corresponds to the origin of axes. The nondimensional current density is calculated by the relationship, $\mathbf{J}=\nabla\times\mathbf{B}$, i.e., by Ampere's law, and the given two-dimensional flow only has the $J_z$ component non-zero. The local Nusselt number at the isothermal sidewalls is calculated from the temperature field as

$$\mathrm{Nu}(Y)=-\left|\frac{\partial\Theta}{\partial X}\right|_{X=0\text{ or }1}\tag{7}$$

The average Nusselt number at the sidewall is given by the relation

$$\mathrm{Nu}=\int_{Y=0}^{1}\mathrm{Nu}(Y)dY\tag{8}$$

### 2.1. Numerical Solution

The governing equations together with the corresponding initial and boundary conditions are solved numerically, employing a finite-volume method. The coupling between momentum and continuity equations is achieved using the SIMPLE method [21] via the so-called pressure-correction equation. A non-uniform staggered grid in

both horizontal and vertical directions is employed to account for steep gradients near the walls. The nonlinear terms of all equations are discretized using the QUICK scheme of Leonard [22] in the stable form proposed by Hayase et al. [23] in order to minimize numerical diffusion. Central differences are used for the diffusion terms and a second-order scheme for the transient terms. The linearized system of equations is solved by the TDMA method. In all calculations presented here, under-relaxation factors with values of 0.5, 0.5, 0.6, 0.6, 0.6, and 0.3 are applied to the $U$, $V$, $B_x$, $B_y$, $\Theta$, and the pressure correction equations, respectively. The iterative procedure at each time step is initiated by solving the Navier-Stokes equations to obtain the velocity and pressure fields, followed by the solution of the energy and magnetic induction equations, and is continued until convergence is achieved. Then the solution is repeated for the next time step, which is obtained for a CFL condition equal to 0.5, until the establishment of a steady-state solution. The numerical scheme permits the identification of transition-to-unsteadiness, and when this happens the calculation is stopped. Convergence is established through the sum of the absolute relative errors for each dependent variable in the entire flow field.

$$\sum_{i,j} \frac{|\varphi_{i,j}^{n+1} - \varphi_{i,j}^{n}|}{|\varphi_{i,j}^{n}|} \leq \epsilon \tag{9}$$

where $\varphi$ represents the variables $U$, $V$, $B_x$, $B_y$, or $\Theta$. The superscript $n$ refers to the iteration number or time step, and the subscripts $i$ and $j$ refer to the space coordinates. The value of the convergence criterion $\epsilon$ is chosen as small as $10^{-6}$ for all calculations which are carried out on Intel CPU based computers. More details about the numerical procedure and code validation may be found in Sarris et al. [24].

The external magnetic field **B** in the presence of the solid boundaries results in the formation of magnetic boundary layers (so called Hartmann and sidewall diffusion layers, see Alboussière and Lingwood [25]). The Hartmann layers develop on walls normal to the magnetic field with thickness proportional to $\mathrm{Ha}^{-1}$, and the sidewall diffusion layers on the parallel walls with thickness proportional to $\mathrm{Ha}^{-1/2}$ [26]. When the Hartmann number is high enough, the magnetic boundary layer may be thinner than the corresponding momentum and thermal boundary layers. For this reason, a cosine distribution for the grid nodes is used in both directions in order to better resolve the boundary layers and to accurately predict the heat transfer at the isothermal walls.

Before the final calculations, a grid independence test was conducted in order to determine the optimum grid. The most convective flow case (i.e., that with the higher Hartmann and Grashof numbers) was selected for this test because of the increasing sensitivity of the nonlinear terms to grid refinement. The calculated field values for a grid size of $128 \times 128$ showed that the maximum streamfunction and the average Nusselt number differ only by less than 0.01% from a double size grid and thus, this grid was considered adequate for the present calculations.

## 3. RESULTS AND DISCUSSION

In the present numerical study, the applied (or resulting as a combination of suitable placed electrodes and permanent magnets) magnetic field produces one of

the driving forces on the electrically-conducting fluid. As a result of this forcing, an MHD flow analogous to the Kolmogorov flow is established in the enclosure [10, 11, 17, 18, 27]. The magnetic force is combined with the buoyant force due to the lateral heated sidewalls of the enclosure. The ranges of values of the flow parameters studied are: Hartmann number $\mathrm{Ha} = 0$ to 100, magnetic force wave number $k = 0$ to 2, and magnetic Reynolds number $R_m = 0.003$ to 0.05, generally corresponding to laminar liquid metal flows in industrial or laboratory scale.

The Grashof number is fixed to the relatively high, but still in the laminar flow regime, value of $\pm 10^6$ and the Prandtl number to the value 0.0321 which is common for liquid metals. The sign $\pm$ in the Grashof number is used to signify the contribution (+) or resistance (−) of the buoyancy force to the flow driven by the magnetic force. The practical meaning of this assumption is connected to the imposed temperature difference of the sidewalls. When the left wall is kept at a higher temperature causing the flow to ascend, the buoyancy force contributes to the rotation due to the magnetic force. In contrast, when the left wall is kept at a lower temperature, the buoyant force resists the magnetic force. A schema of the combined action of the Lorentz and buoyancy forces is presented in Figure 2. For the cases of pure magnetic driving, the Grashof number is considered zero. This corresponds to a zero gravity environment or negligible temperature gradients.



### 3.1. Effect of Hartmann and Grashof Numbers

The increase of the Hartmann number is compatible to the increase of the electric potential in the experiments of Bondarenko et al. [10], Batchaev and Dowzhenko [11], and Honji [17]. Figures 3 and 4 show the distribution of the streamfunction and the isotherms for $R_m = 0.003$ in the cases of $\mathrm{Gr} = 0$, $10^6$, $-10^6$ for three Hartmann numbers of 10, 30, and 100. The wave number $k$ of the imposed magnetic field for all these cases is 1, while in the experiment of Honji [17] a value of $k = 13$ was considered. Thus, the present cases correspond to one primary circulation while in the experiments of reference [17] up to 13 circulations may be found. Figure 3*a* shows the streamfunction distribution for the pure magnetoconvection case, i.e., when $\mathrm{Gr} = 0$ and only the Lorentz force is driving the flow.

The single primary flow circulation, even in the statistical sense as in the turbulent simulations of reference [16], is a major characteristic of the Kolmogorov flow

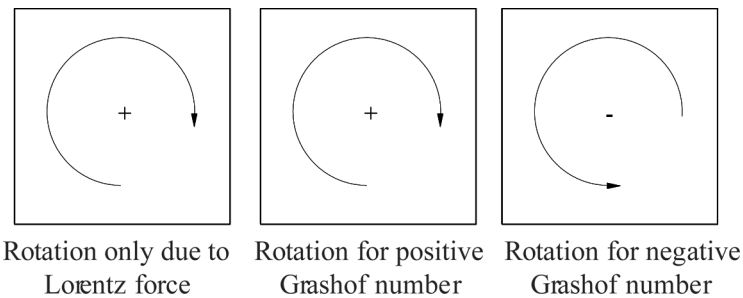


**Figure 2.** Fluid rotation in the enclosure as a result of the applied magnetic or buoyant forcing.

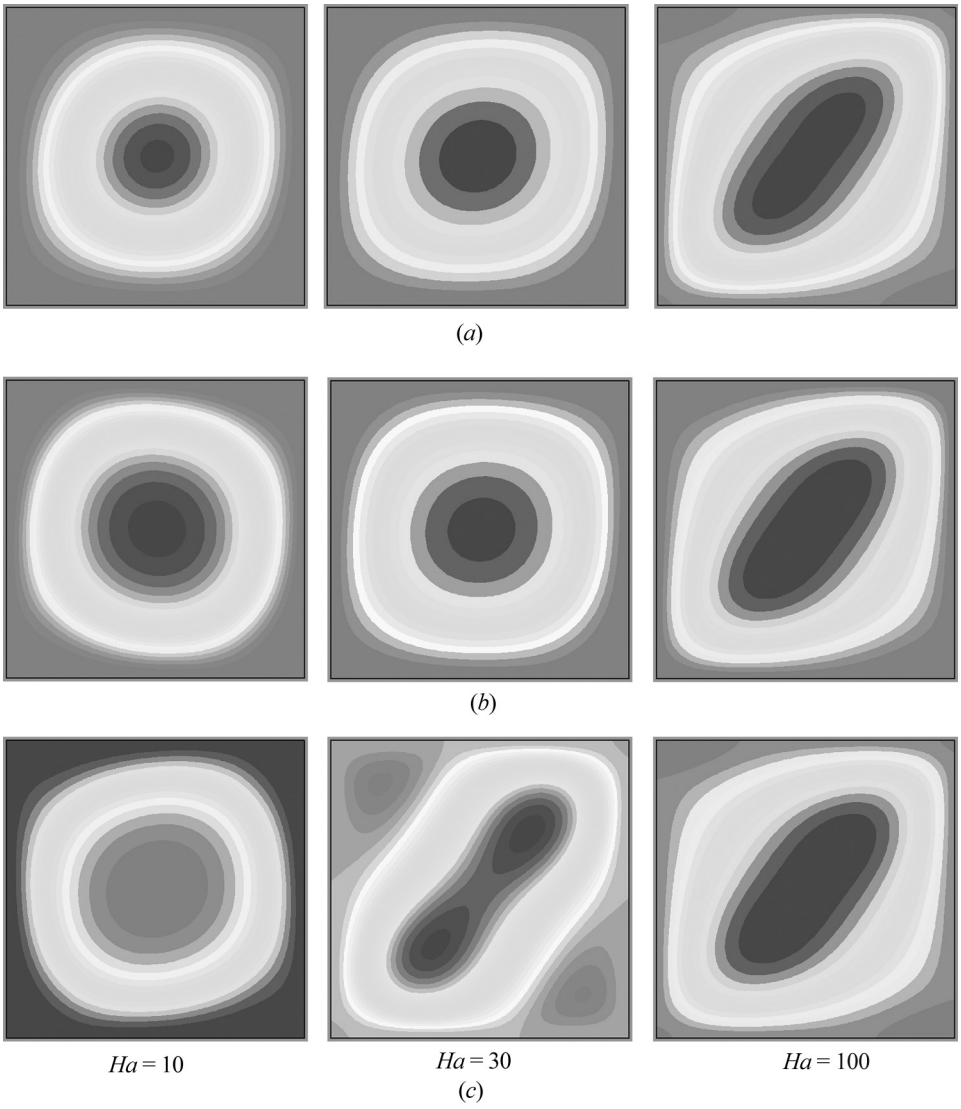


**Figure 3.** Streamfunction distribution for the cases $R_m = 0.003$, Ha = 10, 30, and 100: (*a*) Gr = 0 (−90; −5; −5, −200; −20; −20, −260; −20;0), (*b*) Gr = $10^6$ (−210; −10, −10, −240; −20; −20, −260; −20; −20), and (*c*) Gr = $-10^6$ (10; 10; 140, −40; −2; 6, −240; −20; 0). Numbers correspond to minimum, range, and maximum contour level value.

that exhibits the property of inverse cascade [19, 20] although instabilities can be seeded to longer length scales, i.e., in the shear layers formed by the small vortices near the corners of the enclosure. It is apparent that the flow pattern with the imposed spatially sinusoidal magnetic field is similar to the patterns formed by natural convection (Figures 3*b* and 3*c*). The increase of the Hartmann number above a certain value has a direct influence on the flow pattern resulting in an elongated

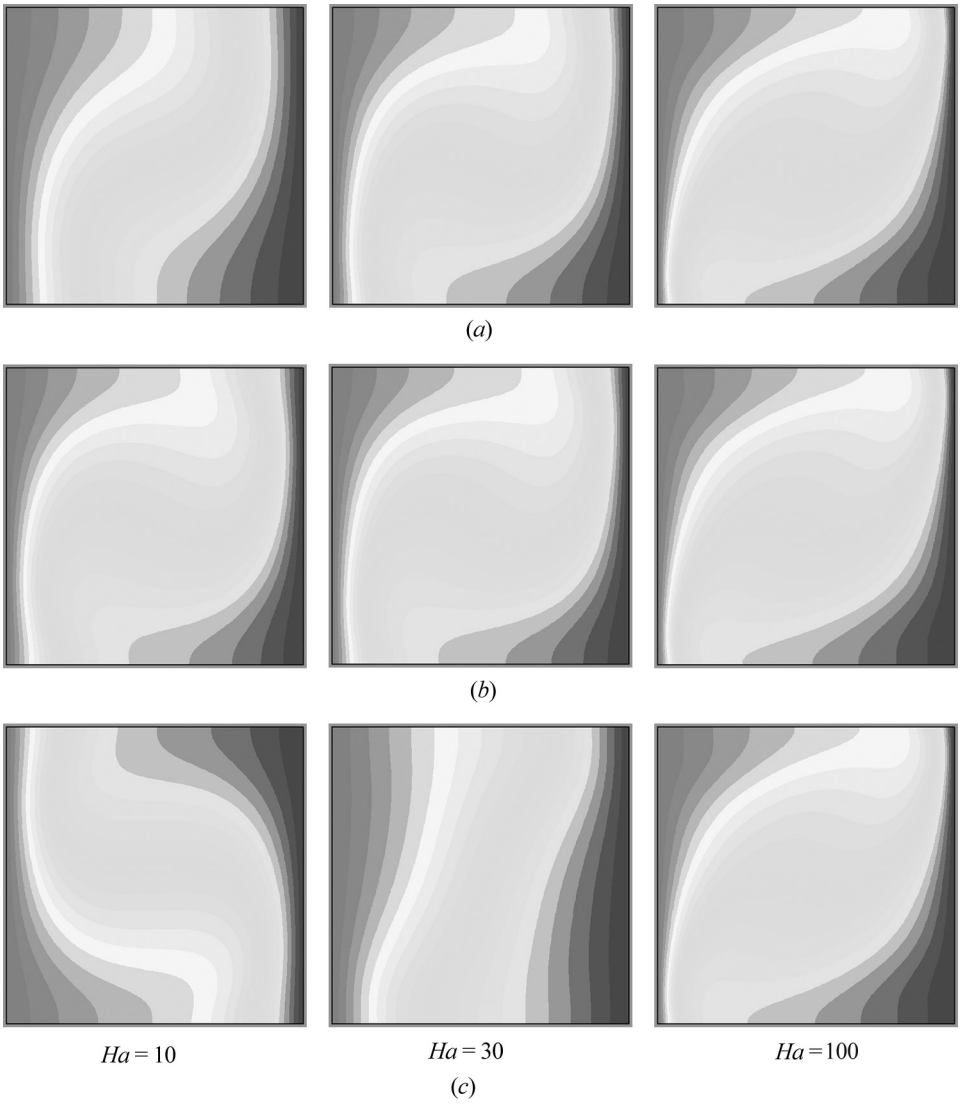


**Figure 4.** Isotherms for the cases $R_m = 0.003$, Ha = 10, 30, and 100: (*a*) Gr = 0, (*b*) Gr = $10^6$, and (*c*) Gr = $-10^6$. The increment of the isotherms is 0.05.

vortex. It is also observed from the curvature of the isotherms close to the walls in Figure 4*a* that the convection heat transfer is significantly enhanced with increasing Hartmann number. This is due to the increase of the magnitude of the driving magnetic force. Thus, the increased magnetic field enhances the heat transfer which is a non-trivial consequence in MHD. In fact, heat transfer enhancement with increasing Hartmann number has only been observed in the case of the formation of turbulent sidewall jets in duct flow [28].

Interesting results are presented in the streamfunction distribution plots of Figures 3*b* and 3*c*, showing the combined flow due to both magnetoconvection and buoyant forces. Thermal convection is the dominant mechanism of fluid flow and heat transfer at small Hartmann numbers, and the direction of flow rotation follows the corresponding temperature difference of the sidewalls (or the sign of the Grashof number as explained above). In general, it is known that the inverse cascade of the Kolmogorov flow is arrested by the relatively weak stratification [19]. However, a primary vortex is always established in laterally-heated enclosures favoring a possible inverse cascade. Thus, both types of flow that coexist here as a result of the magnetoconvection and the thermoconvection forcing can be characterized as (quasi-) two-dimensional even in the transitional or turbulent regimes.

The thermal convective flow for $\mathrm{Gr} = 10^6$ that results in the same clockwise rotation as in the case of only the magnetically-driven flow, is progressively getting stronger with the increase of the Hartmann number. On the other hand, the anticlockwise rotating buoyant flow for $\mathrm{Gr} = -10^6$ is completely reversed for $\mathrm{Ha} = 30$ and acquires the same clockwise rotation as in the case of the pure magnetic forcing. For $\mathrm{Ha} = 100$, the magnetic force has completely dominated the flow for both cases ($\mathrm{Gr} = \pm 10^6$) of buoyant flow studied here. In the analysis of the laminar Kolmogorov flow, the basic circulation pattern is usually a circle [13] even for high wave numbers, while here the vortices are elongated as in the stability analysis of the electromagnetically-driven Kolmogorov flow of Chen and Price [29]. The elongated flow pattern at high Hartmann numbers is characteristic for all MHD flows and are connected to the tendency of the vortices to align with the direction of the external magnetic field. In the present MHD flow, the magnetic field vector is somehow inclined with respect to the Cartesian axes and, thus, the vortex is elongated in the diagonal of the enclosure. The effect of flow reversal and the domination of magnetoconvection heat transfer as the Hartmann number increases is also well illustrated by the isotherms of Figures 4*b* and 4*c*.

The effect of the magnetoconvection on the fluid circulation intensity is shown in Figure 5*a*, where the maximum value of the streamfunction is plotted for various Hartmann numbers. It may easily be concluded that for $\mathrm{Gr} \geq 0$, the increase of the Hartmann number causes the increase of the flow circulation intensity. In contrast, when the buoyant force is in competition with the magnetoconvection ($\mathrm{Gr} < 0$), the increase of Hartmann number makes a progressive domination of the Lorentz force. Initially, the circulation intensity decreases as the two driving forces counteract and the fluid is slowed down, thus favoring conduction heat transfer. For this case, at approximately $\mathrm{Ha} = 30$ a stratification is observed in the flow as a result of the equilibrium between the buoyant and magnetoconvection forces for the particular values of the Grashof and Hartmann numbers. When the flow is reversed, the magnitude of the maximum streamfunction increases again (the negative sign of $\Psi$ in Figure 5*a* corresponds to clockwise rotation) and magnetoconvection heat transfer starts to dominate. For high enough Hartmann numbers the magnitude of the maximum stream function values are comparable for $\mathrm{Gr} = 0$ and $10^6$.

It should also be noted that in all combinations of forcing which is tested here the increase of the Hartmann number to a value above 50 has no direct effect on the circulation intensity maximum value, $\Psi_{\max}$, which remains almost constant. In fact, the flow field for the value of $\Psi_{\max}$ for $\mathrm{Ha} > 50$ does not remain constant, and the

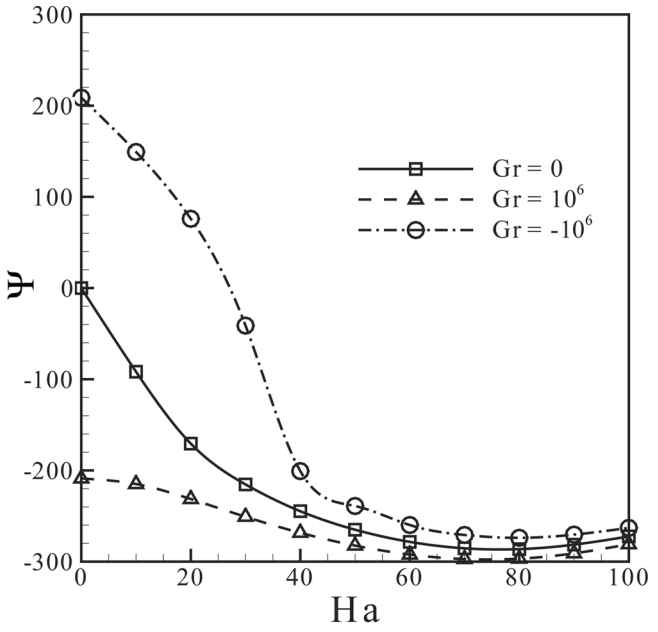


(*a*)

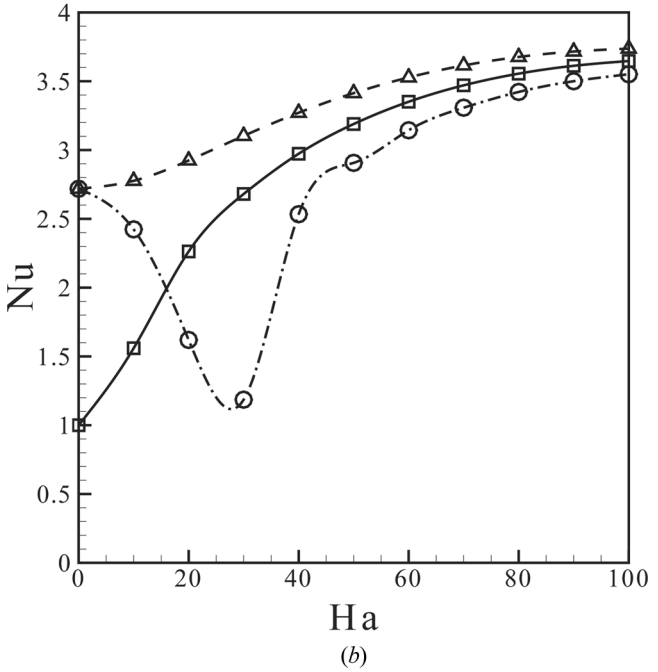


(*b*)

**Figure 5.** Variation of (*a*) the maximum streamfunction, and (*b*) the average Nu with Ha for $Gr = 0$, $10^6$, and $-10^6$. Lines are spline fitting of the point results.

additional kinetic energy due to the increase of the Lorentz force is cascading to secondary vortices. This is connected to the nonlinear nature of the governing equations which have the tendency to favor bifurcations. In particular, the kinetic energy is transferred to the secondary patterns which are formed at the corners of the enclosure. For $Ha > 100$, these bifurcations may become unstable and turbulent convection may be established. This flow regime is not studied here because turbulent models or direct numerical simulations would be needed. Experimental results showing flow patterns arising after the primary shear flow loses its stability can be found in Dolzhanskii et al. [27]. The latter is a similar unstable Kolmogorov shear flow in thin layers where the applicability of the quasi-two-dimensional approximation (similar to Somméria and Moreau [30] for high magnetic fields) is directly verified.

The magnetic driving also affects the convective heat transfer from the sidewalls, as shown in Figure 5*b*, where the variation of the Nusselt number with Hartmann number is presented. It is important to note that the relative increase of the Nusselt number for $Ha = 100$ for the case where both the magnetic and buoyant forces produce the same rotation ($Gr = 10^6$) is of the order of 40% compared to the corresponding natural convection case. This increase of the Nusselt number is essential in the present MHD flow of liquid metals because of the possible technological aspects, especially in fusion blankets where very high magnetic fields exist. In connection to the flow circulation intensities of Figure 5*a*, when the two driving mechanisms are competitive, Figure 5*b* shows that the heat transfer is reduced initially due to the decrease of convection heat transfer and then increases with the Hartmann number.

The asymptotic behavior of the flow circulation intensity for $Ha > 50$ which is discussed above affects the heat transfer less, which is increased with the Hartmann number due to the fact that the heat is mainly transferred through the boundary layers that are formed near the walls. This is confirmed by the present results which show that the increase of the Hartmann number, above a characteristic value, influences mainly the boundary layers and not the core flow. This is also illustrated by the distribution of the electric current and Lorentz force (magnitude of $\mathbf{B}\nabla\mathbf{B}$) in the enclosure for the case of $Ha = 100$ and $Gr = 0$ shown in Figure 6. In particular, this figure shows that stronger electric currents are gathering inside the Hartmann and sidewall diffusion layers, while the magnitude of the Lorentz force in the core flow is almost zero. Only for the higher Hartmann numbers studied here, does the Nusselt number reach a plateau which is probably the limiting value of the Lorentz force for the laminar heat transfer regime before flow transition occurs. The distributions of the magnetic field components $B_x$ and $B_y$ are presented in Figure 6 for this particular case of high Hartmann number.

### 3.2. Effect of Wave and Magnetic Reynolds Number

This part of the study mainly concerns the resulting flow at $Gr = 0$ as the wave number $k$ of the sinusoidal magnetic forcing is increased from 0 to 2 in increments of 0.25. In the experiments of the same flow [10, 11, 17], only an integer increase of the $k$ number was permitted, corresponding to the placing of additional magnetic poles or electrodes. From the present simulations it was found that the flow phenomena observed for $k$ numbers greater than 2 are probably not steady state but rather

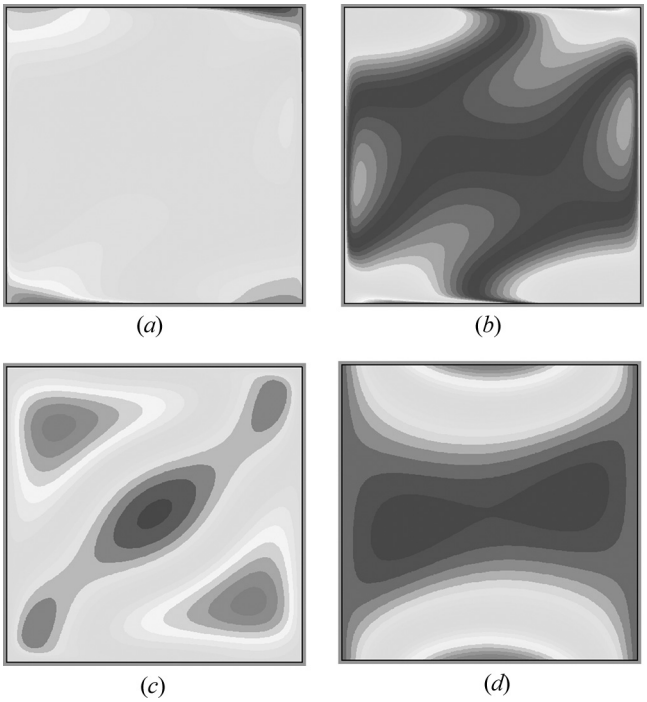


**Figure 6.** Distribution of (*a*) the electric current $J_z$ (−4.5;0.5;4.5), (*b*) the Lorentz force (magnitude of $\mathbf{B}\nabla\mathbf{B}$, 0.2;0.2;5.6), (*c*) $B_x$ (0.925;0.01;1.065), and (*d*) $B_y$ (−0.05;0.05;0.95) for the case of $\mathrm{Ha} = 100$ and $\mathrm{Gr} = 0$. Numbers correspond to minimum, step, and maximum contour level value.



transitional or even turbulent because of the dynamic nature of the shear flow and the vortex breaking (at least for some values of the parameters space studied here). These secondary instabilities are related to an instability of Kolmogorov type [31] in which large-scale disturbances that are transverse to the plane of the periodic flow become unstable. In this secondary instability regime, the system of the governing equations bifurcates to time-dependent solutions with no spatial symmetry.

Figure 7 shows the effect of the $k$ number on the flow for the case $\mathrm{Ha} = 20$, $\mathrm{Gr} = 0$ and $R_m = 0.003$. For $k = 0$ (not shown in Figure 7) no Lorentz force is acting on the flow, while no significant variation of the circulation pattern is observed for values of $k$ up to 1.5. For $k = 1.75$, secondary circulations located at the right corners of the enclosure are growing and the beginning of the formation of a vortex pair is observed due to the action of the Lorentz force. The increase of convection due to the increase of the $k$ number is more obvious in the curvature of the isotherms and their distribution close to the vertical walls. The isotherms for the case $k = 0.25$ are nearly parallel to the isothermal walls due to the domination of conduction heat transfer. Strong curvature of the isotherms and consequently domination of convection is observed for $0.75 < k < 1.75$, while for the case $k = 2$ the vortex breaking and the symmetric vortex pair that is formed is found to be less convective than for the latter cases.

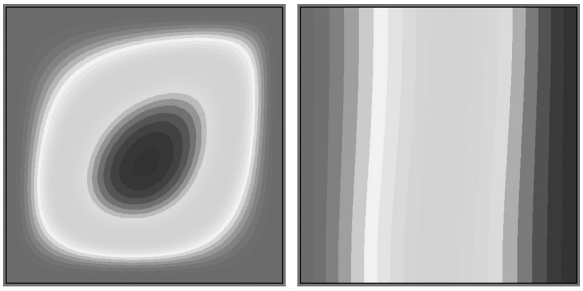

(*a*)

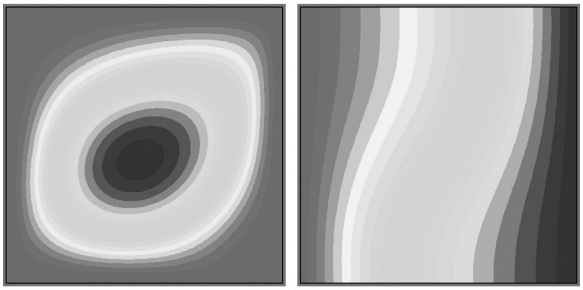

(*b*)

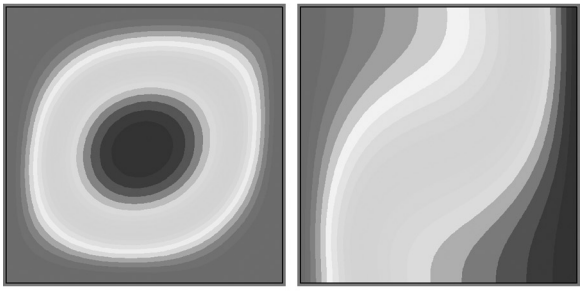

(*c*)

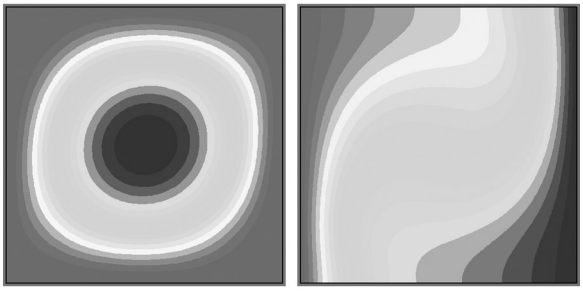

(*d*)

**Figure 7.** Distribution of streamfunction and isotherms for Ha = 20, Gr = 0, and (*a*) $k = 0.25$ (−5.4; −0.2; −0.2), (*b*) $k = 0.5$ (−36; −2; −2), (*c*) $k = 0.75$ (−90; −5; −5), (*d*) $k = 1$ (−160; −10; −10), (*e*) $k = 1.25$ (−210; −10; −10), (*f*) $k = 1.5$ (−200; −10; 0), (*g*) $k = 1.75$ (−130; −10; 0), and (*h*) $k = 2$ (−50; −5; 50). The increment of the isotherms is 0.05. Numbers correspond to minimum, step, and maximum contour level value.

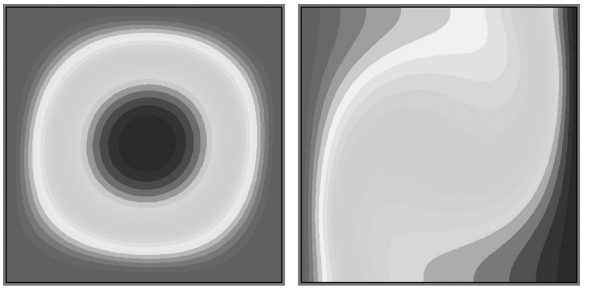

(*e*)

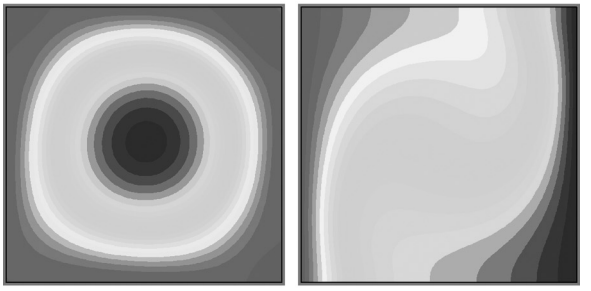

(*f*)

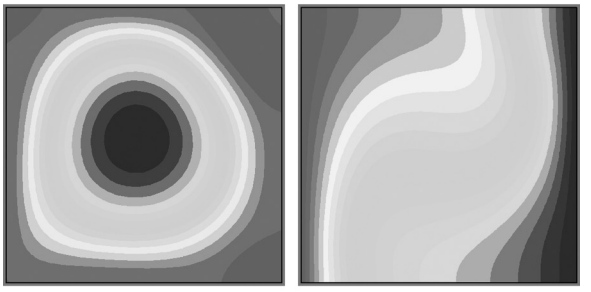

(*g*)

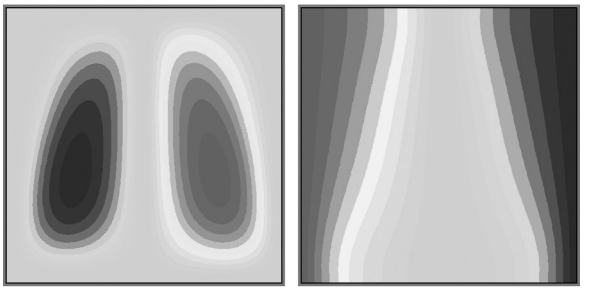

(*h*)

**Figure 7.** Continued.

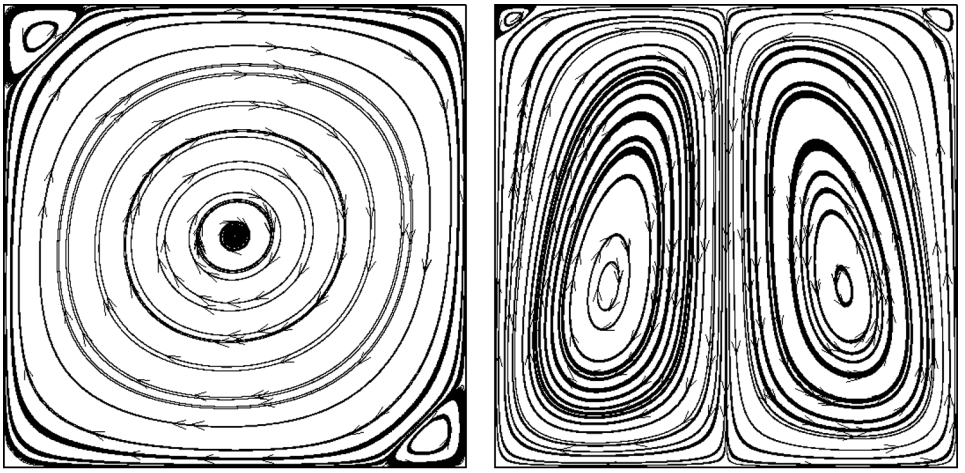

(*a*) (*b*)

**Figure 8.** Streamlines for Ha = 20 and Gr = 0; (*a*) $k = 1$ and (*b*) $k = 2$.

The streamlines of the flow at Gr = 0 for wave numbers $k = 1$ and 2 are presented in Figure 8. As it is expected, the primary flow pattern for $k = 1$ is divided into a pair of circulations when $k = 2$, and this increase of vortices is proportional to the increase of $k$. The structure of the symmetric vortex pair pattern for $k = 2$ has a similar egg-like shape as the one found by Nakamura [18] before transition occurred. In the present case, the entire height of the enclosure is covered by the vortex pair while the vortices of Nakamura [18] were localized at the bottom. This is because the penetration of the magnetic field in the enclosure and the strength of the Lorentz force have a direct influence on the extension of these vortices. This penetration can be seen in the distribution of the Lorentz force in Figure 9 for the cases of $k = 1$ and 2. As $k$ increases the influence of the Lorentz force it is localized closer to the boundary layers. The localized action of the magnetic field (specially of the $B_y$ component) is also presented in Figure 9.

The effect of the wave number $k$ on the flow circulation intensity and the heat transfer at Gr = 0 is presented in Figure 10. The value of the maximum streamfunction $\Psi$ starts from zero at $k = 0$, increases monotonically up to $k = 1.25$, and then decreases. A similar behavior is exhibited by the convective heat transfer from the isothermal walls (indicated by the Nusselt numbers). For values of $k$ greater than 2 and for the parameters considered in the present simulations, the flow is expected to form a more complicated pattern of vortices where the kinetic energy is being distributed further and the heat transfer is reduced for the entire laminar flow regime.

In general for $R_m \ll 1$, advection is relatively unimportant and so the magnetic field will tend to relax towards a purely diffusive state, determined mainly by the boundary conditions. However, it is found sometimes that a small value of the magnetic Reynolds number does not necessarily mean that magnetic diffusion dominates over convection, and the nonlinear magnetic transport may play an important role even when $R_m$ is small [32]. In order to investigate possible deviations from the usual

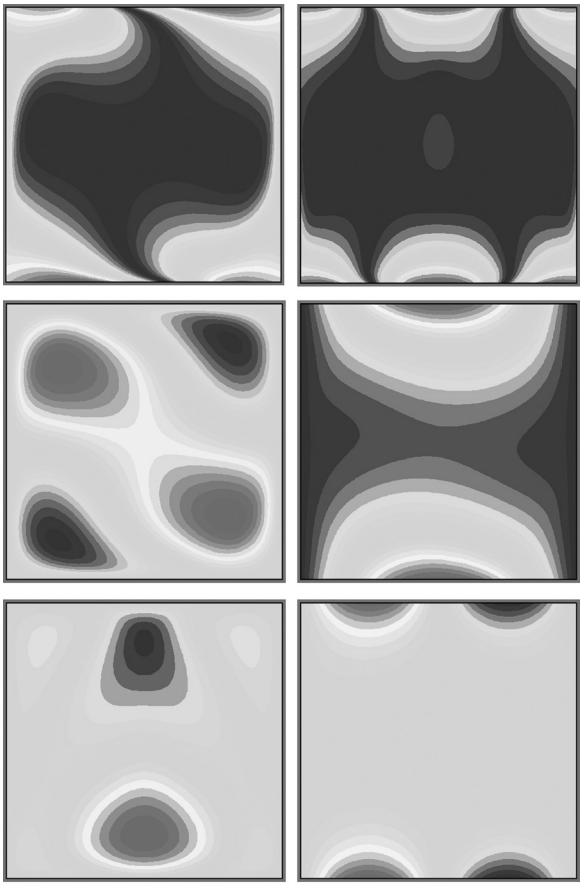


**Figure 9.** Distribution of the Lorentz force (upper), $B_x$ (middle), and $B_y$ (bottom) for the case of $\mathrm{Gr} = 0$, $\mathrm{Ha} = 20$; (*a*) $k = 1$ (0.2; 0.2; 3.8,0.95; 0.005; 1.055,0.05; 0.05; 0.95), and (*b*) $k = 2$ (0.5; 0.5; 6.5,0.965; 0.005; 1.035, −0.9; 0.1; 0.9). Numbers correspond to minimum, step, and maximum contour level value.



effect of the magnetic Reynolds number on the liquid metal flow (especially as here under the effect of spatially-varied boundary conditions and possible transition to turbulence), we studied the range of $R_m < 1$ which covers liquid metal flows in industrial or laboratory scale [24], as described below.

Figure 11 shows the distribution of the maximum streamfunction and Nusselt number at various magnetic Reynolds numbers and $\mathrm{Gr} = 0$ as a function of the Hartmann number. The decrease of $R_m$ results to an increase of the circulation intensity and consequently to an increase of heat transfer from the isothermal walls. As it may be observed, for high enough Hartmann numbers both the circulation intensity and the heat transfer remain almost constant. The values of the above quantities depend only on the value of the magnetic Reynolds number because of its connection to the magnitude of the Lorentz force.

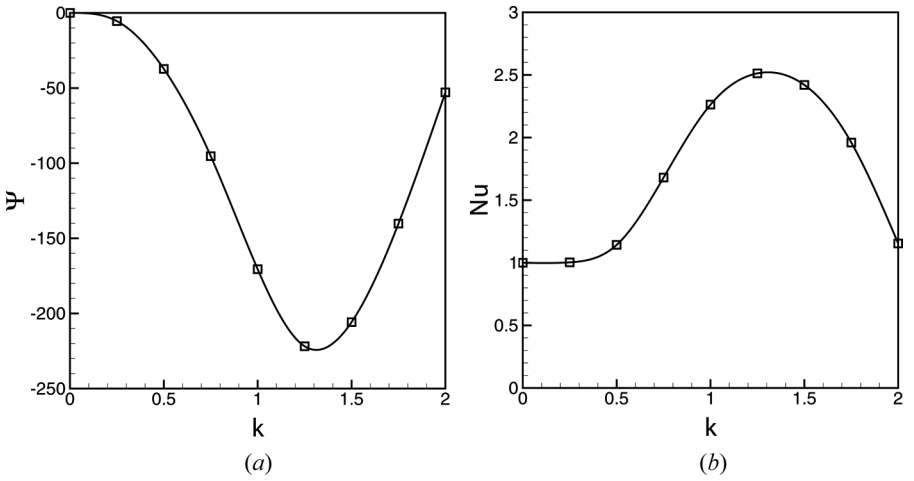


**Figure 10.** Variation of (*a*) the maximum streamfunction for Gr = 0, and (*b*) the average Nu with $k$ wave number. Lines are spline fitting of the calculated points.

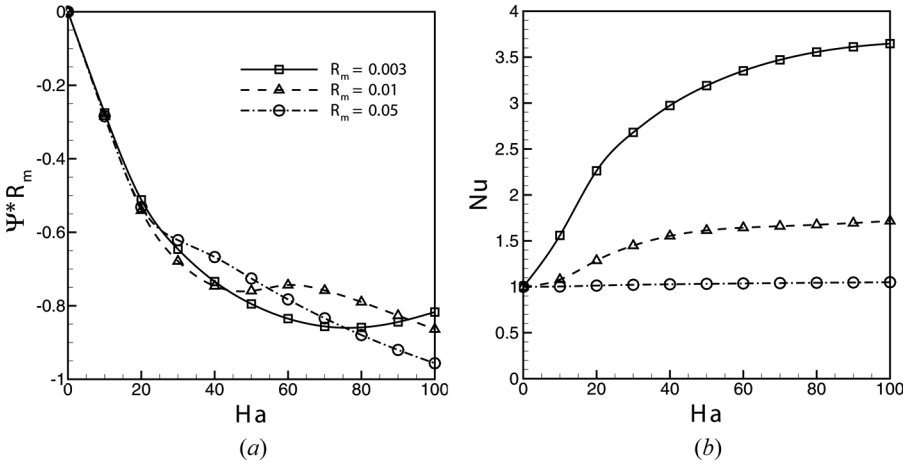


**Figure 11.** Variation of (*a*) the maximum streamfunction (multiplied by $R_m$), and (*b*) the average Nu with Ha number for $R_m = 0.003$, 0.01, and 0.05. Lines are spline fitting of the calculated points.

## 4. CONCLUSIONS

The laminar regime of free convection flow due to spatially varying magnetoconvection and to thermoconvection in a square enclosure has been numerically studied. It is found that a suitable combination of the magnetic and gravitational forces may enhance heat transfer up to 40% over the usual natural convection heat transfer rates. A stratification of the flow may happen when the two forces have an opposing action on the fluid. For the range of flow parameters considered here, the intensity of the flow circulation and the heat transfer reach asymptotically a

plateau because the limit of transition-to-unsteadiness is reached for large enough Hartmann numbers.

An important parameter of the current sinusoidal forced flow is the wave number that determines the number of periods of the external Lorentz force along the enclosure walls. The increase of the wave number $k$ increases the circulation intensity and enhances heat transfer, for $k > 1.25$, both the circulation intensity and the heat transfer decrease due to the breaking of the main flow pattern. This study was restricted to values of $k \leq 2$ before flow transition was reached ($k > 2$). The magnetic Reynolds number was found to be a significant flow parameter since it controls the portion of the magnetic energy that will be transformed into fluid kinetic energy.

## REFERENCES


1. H. Ozoe and K. Okada, The Effect of the Direction of the External Magnetic Field on the Three-Dimensional Natural Convection in a Cubical Enclosure, *Int. J. Heat Mass Transfer*, vol. 32, no. 10, pp. 1939–1954, 1989.
2. R. Mössner and U. Müller, A Numerical Investigation of Three-Dimensional Magnetoconvection in Rectangular Cavities, *Int. J. Heat Mass Transfer*, vol. 42, no. 6, pp. 1111–1121, 1999.
3. S. Kenjereš and K. Hanjalić, Numerical Simulation of Magnetic Control of Heat Transfer in Thermal Convection, *Int. J. Heat Fluid Flow*, vol. 25, no. 3, pp. 559–568, 2004.
4. K. Hanjalić and S. Kenjereš, T-RANS Simulation of Deterministic Eddy Structure in Flows Driven by Thermal Buoyancy and Lorentz Force, *Flow, Turbulence and Combustion*, vol. 66, no. 4, pp. 427–451, 2001.
5. H. B. Hadid, D. Henry, and S. Kaddeche, Numerical Study of Convection in the Horizontal Bridgman Configuration under the Action of a Constant Magnetic Field, Part 1. Two-dimensional flow, *J. Fluid Mech.*, vol. 333, pp. 23–56, 1997.
6. L. N. Hjellming and J. S. Walker, Melt Motion in a Czochralski Crystal Puller with an Axial Magnetic Field: Motion Due to Buoyancy and Thermocapillarity, *J. Fluid Mech.*, vol. 182, pp. 335–368, 1987.
7. K. F. Wu and J. P. Brancher, Thermoconvective instability in a Bounded Vertical Cylinder with Internal Heat Generation, *Int. J. Heat Mass Transfer*, vol. 43, pp. 3775–3784, 2000.
8. P. A. Davidson, *An Introduction to Magnetohydrodynamics*, Cambridge Univ. Press, Cambridge, 2001.
9. N. B. Morley, S. Smolentsev, L. Barleon, I. R. Kirillov, and M. Takahashi, Liquid Magnetohydrodynamics - Resent Progress and Future Direction for Fusion, *Fusion Eng. and Design*, vol. 51–52, pp. 701–713, 2000.
10. N. F. Bondarenko, M. Z. Gak, and F. V. Dolzhansky, Laboratory and Theoretical Models of a Plane Periodic Flow, *Izv. Akad. Nauk (Fiz. Atmos. Okeana)*, vol. 15, pp. 1017–1026, 1979. (in Russian)
11. A. M. Batchaev and V. A. Dowzhenko, Experimental Modeling of Stability Loss in Periodic Zonal Flows, *Dokl. Akad. Nauk*, vol. 273, pp. 582, 1983. (In Russian)
12. A. M. Obukhov, Kolmogorov Flow and Laboratory Simulation of It, *Russ. Math. Surv.*, vol. 38, no. 4, pp. 113–126, 1983.
13. A. Thess, Instabilities in Two-Dimensional Spatially Periodic Flows, Part I: Kolmogorov Flow, *Phys. Fluids A*, vol. 4, pp. 1385–1395, 1992.
14. V. Borue and S. A. Orszag, Numerical Study of Three-Dimensional Kolmogorov Flow at High Reynolds Numbers, *J. Fluid Mech.*, vol. 306, pp. 293–323, 1996.

15. J. V. Shebalin and S. L. Woodruff, Kolmogorov Flow in Three Dimensions, *Phys. Fluids*, vol. 9, pp. 164–170, 1997.
16. I. E. Sarris, H. Jeanmart, D. Carati, and G. Winckelmans, Box-size Dependence and Breaking of Translational Invariance in the Velocity Statistics Computed from Three-Dimensional Turbulent Kolmogorov Flows, *Phys. Fluids*, vol. 19, pp. 095101, 2007.
17. H. Honji, Instability of an Electromagnetically Driven Vortex Array, *Proc. Sixth Asian Congress of Fluid Mechanics Nanyang Technological Univ.*, Singapore, pp. 1218–1221, 1995.
18. Y. Nakamura, Spatio-Temporal Dynamics of Forced Periodic Flows in a Confined Domain, *Phys. Fluids*, vol. 9, pp. 3275–3287, 1997.
19. N. J. Balmforth and Y. N. Young, Stratified Kolmogorov Flow, *J. Fluid Mech.*, vol. 450, pp. 131–167, 2002.
20. N. J. Balmforth and Y. N. Young, Stratified Kolmogorov Flow, Part 2, *J. Fluid Mech.*, vol. 528, pp. 23–42, 2005.
21. S. V. Patankar, *Numerical Heat Transfer and Fluid Flow*, Hemisphere, London, 1980.
22. B. P. Leonard, A Stable and Accurate Convective Modelling Procedure Based on Quadratic Upstream Interpolation, *Comp. Methods Appl. Mech. Eng.*, vol. 19, pp. 59–98, 1979.
23. T. Hayase, J. A. C. Humphrey, and R. Greif, A Consistently Formulated QUICK Scheme for Fast and Stable Convergence using Finite-Volume Iterative Calculation Procedure, *J. Comput. Physics*, vol. 98, pp. 108–118, 1992.
24. I. E. Sarris, G. K. Zikos, A. P. Grecos, and N. S. Vlachos, On the Limits of Validity of the Low Magnetic Reynolds Number Approximation in MHD Natural Convection Heat Transfer, *Numeri. Heat Transfer, B*, vol. 50, no. 2, pp. 157–180, 2006.
25. T. Alboussière and R. J. Lingwood, A Model for the Turbulent Hartmann Layer, *Phys. Fluids*, vol. 12, no. 6, pp. 1535–1543, 2000.
26. R. Moreau, *Magnetohydrodynamics*, Kluwer Academic Press, London, 1998.
27. E. V. Dolzhanskii, V. A. Krymov, and D. Y. Manin, An Advanced Experimental Investigation of Quasi-Two-Dimensional Shear Flows, *J. Fluid Mech.*, vol. 241, pp. 705–122, 1992.
28. U. Burr, L. Barleon, U. Müller, and A. Tsinober, Turbulent Transport of Momentum and Heat in Magnetohydrodynamic Rectangular Duct Flow with Strong Sidewall Jets, *J. Fluid Mech.*, vol. 406, pp. 247–279, 2000.
29. Z. M. Chen and W. G. Price, Secondary Fluid Flows Driven Electromagnetically in a Two-Dimensional Extended Duct, *Proc. Royal Society A*, vol. 461, pp. 1659–1683, 2005.
30. J. Sommèria and R. Moreau, Why, How, and When MHD Turbulence Becomes Two-Dimensional, *J. Fluid Mech.*, vol. 241, pp. 507–518, 1982.
31. J. S. A. Green, Two-dimensional Turbulence Near the Viscous Limit, *J. Fluid Mech.*, vol. 62, pp. 273–287, 1974.
32. J. E. Allen, A Note on the Magnetic Reynolds Number, *J. Physics D: Appl. Phys.*, vol. 19, pp. L133–L135, 1986.